Discrete signal transforms as a tool for processing and analyzing pulsed thermographic data

Ibarra-Castanedo C., González D., Galmiche F., Maldague X. P., Bendada A.
Computer Vision and Systems Laboratory, Dept. of Electrical and Computer Engineering
Université Laval, Quebec City, Canada, G1K 7P4.

ABSTRACT

In this paper, we review some of the discrete signal transforms that are in use in the field of thermography for defect detection and/or characterization. Signal transformation is used with the purpose of finding an alternative domain where data analysis is more straightforward. For instance, it is possible to pass from the time domain to the frequency spectra through the one-dimensional discrete Fourier transform (DFT). The DFT constitutes the basis of pulsed phase thermography (PPT) [1], but other transformations are possible such as the discrete wavelet transform (DWT) [2] with the advantage that, in this case, time information is preserved after the transformation. It is also possible to rearrange data into domains others than frequency. For instance, the Hough transform (HT) allows the detection of regular forms (*e.g.* lines, curves, etc.) in a parameter space. The HT has been used in two different ways in thermography: for the detection of lines in thermal profiles, with the goal of discriminating between defective and non-defective regions [3]; or it can be used to locate the inflection points in phase profiles obtained by PPT to extract the blind frequencies [4]. The Laplace transform can also be used in the time domain to improve flaws detection and their characterization in the transformed space [5]. Eigenvector-based transforms, such as singular value decomposition (SVD), have also been implemented. Principal component thermography (PCT) uses SVD to decompose thermographic data into a set of orthogonal modes [6]. We discuss all these transforms and provide some comparative results.

Keywords: Pulsed thermography, signal processing, Fourier transform, wavelet transform, Laplace transform, Hough transform, singular value decomposition.

1. INTRODUCTION

Pulsed thermography is carried out as depicted in Figure 1, *i.e.* after a thermal pulse ❶ is sent to the surface of the specimen ❷, thermal changes on the surface are recorded with an infrared camera ❸. Data is stored as large 3D matrices containing both spatial (*x*-*y* coordinates) and temporal (*z* coordinate) information ❹, and processed ❺ (*e.g.* through the Fourier transform). Data is usually processed in two ways: (1) at the pixel level as 1D vectors through time; and/or (2) as 2D matrices (images or *thermograms*) at a particular time. In this paper, we present five techniques that are currently used to convert 1D temporal data into a transformed space and we discuss how this transformation is beneficial for defect visualization and characterization.

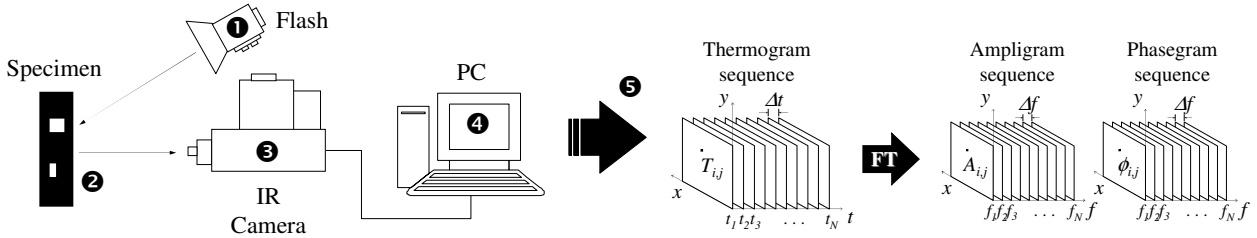

Figure 1. Data acquisition system in pulsed thermography: ❶ thermal excitation; ❷ heat propagation through the specimen; ❸ thermogram recording; ❹ data recording; and ❺ processing, *e.g.* with the Fourier transform.

We begin our discussion with the Fourier transform, which is by far the most commonly used transform in the field of signal processing and which constitutes the basis of pulsed phase thermography (PPT).

2. THE FOURIER TRANSFORM

2.1. Theory

The Fourier transform (FT) is a valuable tool in signal and image processing that gives us access to an alternative (*e.g. frequency*) space. The main interest is either to simplify data analysis or to reduce the amount of computational effort (*e.g.* image compression). The idea behind the FT is that it is possible to reconstruct any 1D function at a particular space (*e.g.* temperature evolution in time) as a summation of sinusoidal terms of increasing frequency. Sinusoids are used since they possess an interesting property that is not observed in any other waveform, *i.e.* a sinusoidal input to the system will produce a sinusoidal output (*sinusoidal fidelity*). This means that, after decomposing the signal in the time domain into sinusoids, the frequency and the waveform will be the same at the output and each one of the resulting terms in the frequency space will differ only in *amplitude A*, and *phase* ϕ.

The discrete FT (DFT) can be written in its complex form as follows [7, 8, 9]:

$$F_n = \Delta t \sum_{k=0}^{N-1} T(k\Delta t)\exp^{(-j2\pi nk/N)} = \mathrm{Re}_n + \mathrm{Im}_n \quad \Rightarrow \quad A_n = \sqrt{\mathrm{Re}_n^2 + \mathrm{Im}_n^2} \qquad \text{and} \quad \phi_n = \tan^{-1}\left(\frac{\mathrm{Im}_n}{\mathrm{Re}_n}\right) \tag{1}$$

where j^2=-1, n designates the frequency increment (n=0,1,…N); Δt is the sampling interval; *Re* and *Im* are the real and the imaginary parts of the transform, respectively. The fast Fourier transform algorithm (FFT) available in MATLAB®: `fft(...)`, allows processing the signal more effectively. Real and imaginary parts of Eq. (1) can be used to calculate the discrete amplitude A_n, and the discrete phase ϕ_n of the transform and to reconstruct 3D matrices as illustrated in Figure 1. This is called pulsed phase thermography [1].

2.2. Pulsed phase thermography using the Fourier transform

Figure 2a presents a typical temperature profile for a pixel from the thermogram matrix in Figure 1 following a pulsed thermography experience. As seen in Figure 2b and c, this kind of function (real) will produce an amplitude and phase response that are even and odd, respectively, with respect to f=0 Hz (*i.e.* $n=N/2$) after the application of the FT. Therefore, from a sequence of N thermograms, there are $N/2$ useful frequency components; the other half of the spectra only provides redundant information and can thus be safely discarded. Hence, the whole data sequence can be processed with the FT so amplitude and phase sequences can be reconstructed.

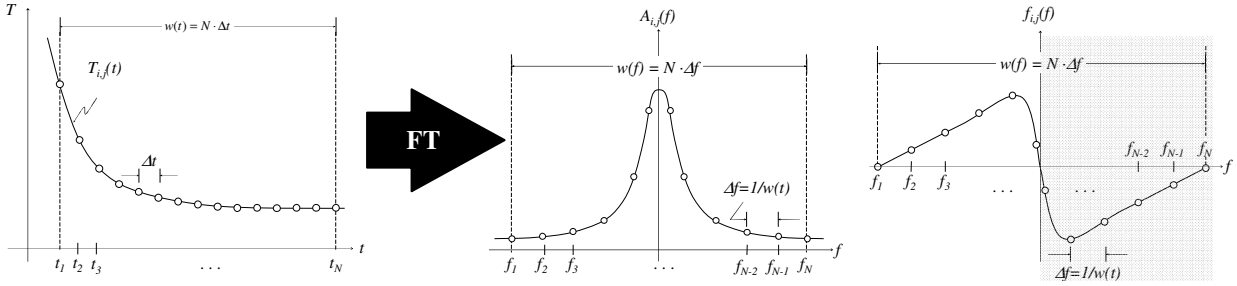

(a) **(b)** **(c)**

Figure 2. (a) Temperature; (b) amplitude; and (c) phase profiles for a pixel on the frequency spectra for a non-defective pixel on coordinates (*i,j*) as indicated in Figure 1.

The interesting aspect of working in the frequency space is that problems such as emissivity variations in the surface, reflections from the environment, non-uniform heating, and surface shape variations, which typically affect pulsed thermal data, have a considerable lesser impact on the phase, therefore, defect contrast is improves. This is true for data coming from a lock-in thermography experience [10, 11] as well as from PPT [12]. PPT has the advantage that an entire phase profile becomes available from a single experience, provided that data is correctly sampled and truncated [13]. Furthermore, a depth inversion procedure using phase data from PPT has been recently proposed [12].

2.3. Depth inversion with the phase

Figure 3 depicts the phase and phase contrast profiles for the case of thick defects (flat-bottomed holes) at two different depths. The phase profiles for the positive part of the spectra for two defects at different depths (ϕ_{z_1}, ϕ_{z_2}), and for a sound area (ϕ_{z_s}), are shown at the bottom part of this graph. Phase contrast ($\Delta\phi_{z_1}$, $\Delta\phi_{z_2}$) can be calculated from the phase profiles as: $\Delta\phi=\phi_d-\phi_{Sa}$, where ϕ_d is the phase of a defective pixel, and ϕ_{Sa} is the phase for a non-defective pixel. The negative value for the phase contrast is used for convenience. Defects are visible (*i.e.* $\Delta\phi>0$) from f=0 Hz to a given frequency, named the *blind* frequency f_b, *i.e.* the frequency at which the phase contrast is enough for a defect to be visible, which is lower for deeper defects ($f_{b,z_1} > f_{b,z_2}$). Phase profiles for defective pixels merge with the phase profile for a sound area into a straight line for frequencies higher than the corresponding blind frequencies ($f > f_b$). Consequently, shallow defects have a larger frequency range of visibility than deep defects.

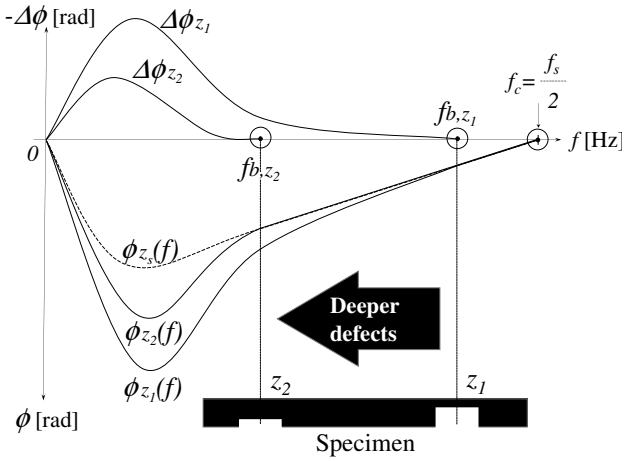

Figure 3. Depth quantification with the phase contrast and blind frequency.

A linear relationship exists between defect depth z, and the inverse square root of the *blind* frequency, *i.e.* $f_b^{1/2}$. The thermal diffusion length expressed by [10]: $\mu=(2\alpha/\omega)$ with $\alpha=k/\rho c_P$ being the thermal diffusivity and $\omega=2\pi f$ the angular frequency, can be used to fit experimental data [12]:

$$z = C_1\sqrt{\frac{\alpha}{\pi\ f_b}} + C_2 \tag{2}$$

where reported values for C_1 are around 1 for amplitude data, and between 1.5 and 2 (when working with phase data obtained by photoacoustics [10] and lock-in thermography [11]), with a value of 1.8 typically adopted. The regression constant C_2 gives an indication of the fitting error.

The phase contrast defined above can be used to determine f_b, although automatic determination without the need of a sound area definition is also possible [12]. Figure 4 shows the depth inversion results using two steel plates with flat-bottom holes (30x30 mm^2) at different depths ranging from 1 to 4.5 mm as indicated [14].

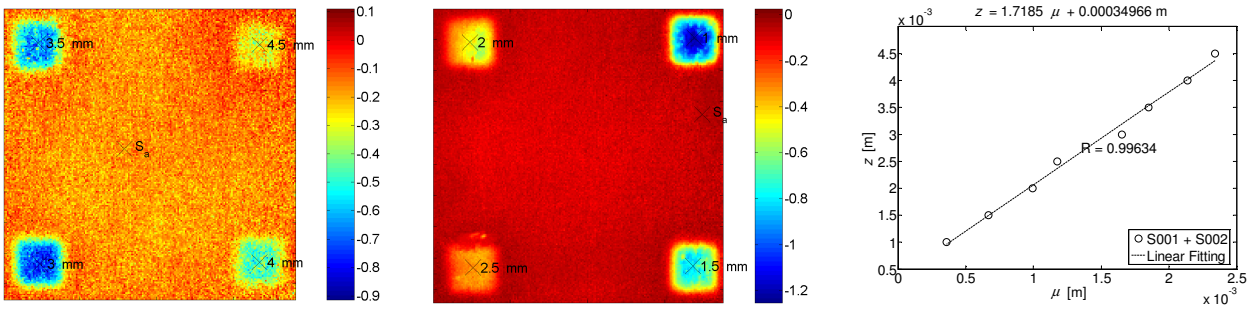

(a) **(b)** **(c)**

Figure 4. Depth inversion results for two steel plates with 4 flat-bottom holes each (30x30 mm^2) at different depths ranging from 1 to 4.5 mm as indicated. Phasegrams at f=0.27 Hz for specimen (a) S001; and (b) S002; and correlation results using Eq. (2). Data from [14]. See color figures on last page.

Phasegrams from both specimens are shown at the left and the correlation results from Eq. (2) are presented on the right. As can be seen from Figure 4c, the depth z, is highly correlated to the diffusion length μ, and the slope of the regression (C_1=1.72) is in agreement to previously reported values (*i.e.* $1.5 < C_1 < 2$).

3. THE WAVELET TRANSFORM

3.1. Theory

As mentioned in the previous paragraph, the FT uses a series of infinite sinusoidal waves to reconstruct *any* type of signal. Nevertheless, this way of representing a function can cause some problems when the signal contains transient components and/or sharp variations. The wavelet transform (WT) was intended as an alternative transformation algorithm to better represent transient functions. Instead of using waves (*e.g.* the sinusoids) as in the FT, the WT uses *wavelets* (*i.e.* waves of limited duration) as its basis functions. The use of wavelets allows processing the information at different *scales* (or *resolutions*) by decomposing the signal into *stretched* and *scaled* replicas of a base wavelet, which allows a better approximation of sharp functions. Furthermore, contrary to the FT, the transformed space after the application of the WT does not contain a frequency coordinate; but rather a *scale-time* joint representation. This time preservation characteristic of the WT is of great interest for quantitative evaluations since depth is directly linked to time.

The continuous WT of a function $f(t)$ can be written as [15]:

$$W_f(S,T) = \int_{-\infty}^{+\infty} f(t) h_{ST}^{*}(t)\,dt = \mathrm{Re} + j\,\mathrm{Im} \tag{3}$$

where W_f denotes the WT, T is the translation factor, S is the scaling factor, and h_{ST} is the daughter wavelet defined from the mother wavelet h:

$$h_{ST}(t) = \frac{1}{\sqrt{S}} h\left(\frac{t-T}{S}\right) \quad \text{and} \quad h(t) = e^{(j\omega_0 t)} e^{\left(-t^2/2\right)} \tag{4}$$

where ω_0 provides the size of the Morlet wavelet $h(t)$ chosen here as the mother wavelet.

The discrete WT (DWT) is in fact, the continuous WT evaluated at discrete scales and translations. Function `dwt(...)` from MATLAB® can be used for this matter. Both real and imaginary parts become available, as seen on equation (3), so that phase and amplitude images can be computed as in the case of the FT.

3.2. Quantitative pulsed phase thermography using the wavelet transform

Figure 5 presents the phasegrams obtained using the DWT at different scaling factors for a CFRP specimen with impact damage. Phasegram in Figure 5a corresponds to a damage zone near the surface. Deeper defect features are revealed gradually for increasing translation factors from Figure 5b to d. From these results, it is possible to provide a direct inversion of the defect depth for a given S through the calibration of T, using phase data obtained with the WT.

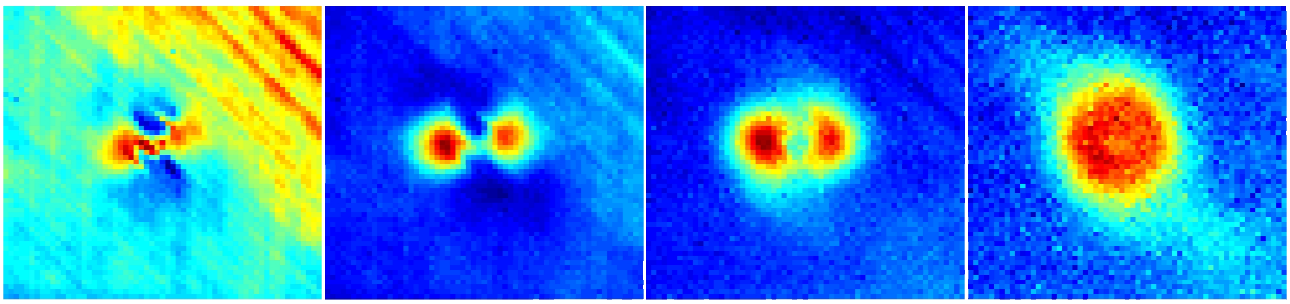

(a) **(b)** **(c)** **(d)**

Figure 5. Relationship between the depth z and the translation factor through the phase using the WT: T= (a) 1.2; (b) 1.8; (c) 2.4 and (d) 3. Impact damage on a CFRP specimen. See color figures on last page.

Figure 6 shows the phasegrams for a 1 and 3 mm depth defects (flat-bottom holes in aluminum) and the regression results for T vs. z at 8 different depths. As can be seen, defects are clearly visible and data is highly correlated.

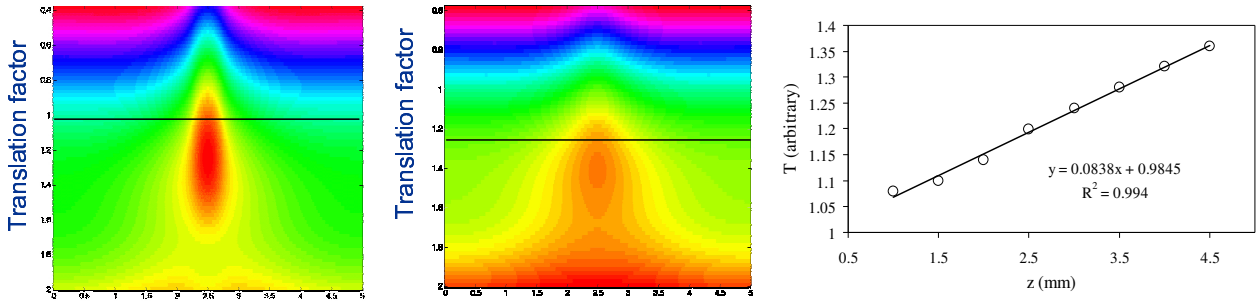

(a) **(b)** **(c)**

Figure 6. Correlation results for an aluminum specimen with flat-bottomed holes: phasegrams as a function of T for a line passing over the defect center at z= (a) 1 mm; (b) 3 mm; and (c) correlation results using all the inspected depths.

4. SINGULAR VALUE DECOMPOSITION

4.1. Theory

As explained above, the FT provides a valuable tool to decompose signal in the *temperature-time* space to a *phase-frequency* space but it does so through the use of sinusoidal basis functions, which may not be the best choice for representing transient signals (as the temperature profiles typically found in pulsed thermography). Singular value decomposition (SVD) is an alternative tool to extract spatial and temporal data from a matrix in a compact or simplified manner. Instead of relying on a basis function, SVD is an eigenvector-based transform that form an *orthonormal* space. Lets assume data are represented as a *MxN* matrix **A** (*M*>*N*), then the SVD allows writing [6]:

$$A=URV^T \tag{5}$$

with **R** being a diagonal *NxN* matrix (with singular values of **A** present in the diagonal), **U** is a *MxN* matrix, $\mathbf{V}^T$ is the transpose of an *NxN* matrix (characteristic time). A singular value decomposition function, `svd(...)` is available in MATLAB®.

The operation in Eq. (5) is illustrated in Figure 7. The columns of **U** represent a set of orthogonal statistical modes known as empirical orthogonal functions (EOF) describing spatial variations of data [6]. On the other hand, the principal components (PCs), representing the time variations, are arranged row-wise in matrix $\mathbf{V}^T$. As will be pointed out below, this characteristics of the SVD approach are very useful for pulsed thermography applications.

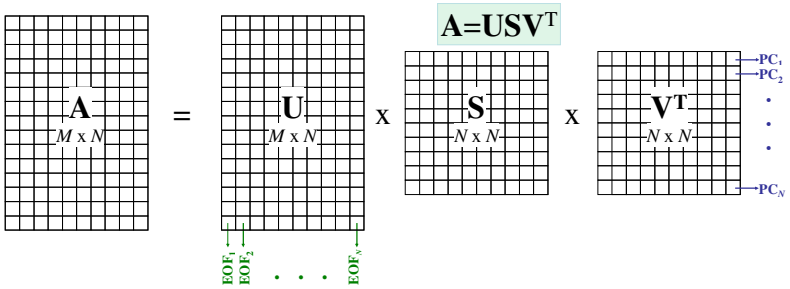

Figure 7. Singular value decomposition of matrix **A** into matrices **U**, **S** and $\mathbf{V}^T$.

4.2. Principal component thermography

Principal component thermography (PCT) [6, 19] uses SVD to extract the spatial (EOFs) and temporal (PCs) information from a thermogram matrix. The thermographic 3D matrix needs to be rearranged as a 2D matrix with time

along the columns and space as illustrated in Figure 8a. After applying the SVD to the 2D matrix, the resulting **U** matrix, providing the spatial information, can be rearranged as a 3D sequence as illustrated in Figure 8b.

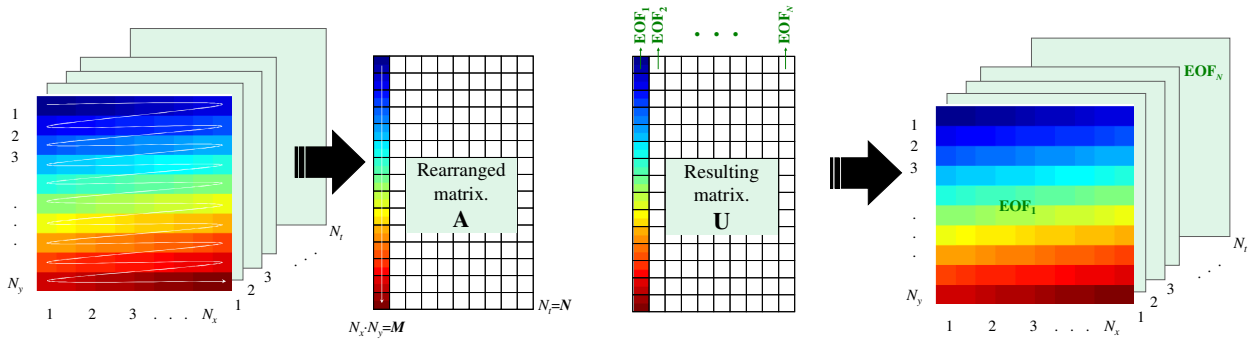

Figure 8. (a) Thermographic data rearrangement from a 3D sequence to a 2D **A** matrix in order to apply SVD; and (b) rearrangement of 2D **U** matrix into a 3D matrix containing the EOFs. See color figures on last page.

Figure 9 shows the first five EOFs for a cropped portion of a 10 plies CFRP specimen with 25 Teflon® inclusions obtained after applying PCT [18]. The inclusions, ranging from 3 to 15 mm in lateral size, are distributed in rows having the same depth (from top to bottom: z=1.0, 0.6, 0.2, 0.4 and 0.8 mm). Two cases are considered: data with no preprocessing (vignetting, fixed pattern noise) at the top row, and preprocessed data with cold image subtraction at the bottom. Later EOFs show mostly noise. For the uncorrected case, the first image (EOF_1) shows the vignetting effect and the fixed pattern noise (FPN). The FPN is still present at the second image (EOF_2), but it no longer shows any vignetting, non-uniform heating shows up instead. Interestingly, the next three EOFs do not present any of these degradation sources, only defects and the specimen fiber matrix are seen.

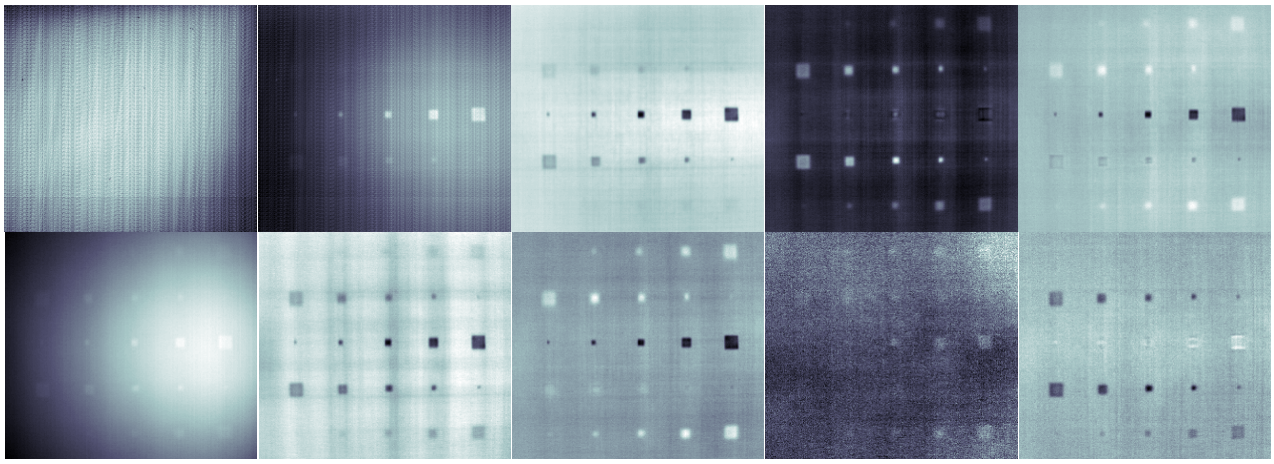

Figure 9. PCT results for the case of uncorrected data (top), and for preprocessed data (bottom) with cold image subtraction: (a) EOF_1; (b) EOF_2; (c) EOF_3; (d) EOF_4; and (e) EOF_5.

From these three images it is possible to detect 22 of the 25 inclusions. For the case when PCT is applied to preprocessed data, there is no vignetting or FPN but is still strongly affected by non-uniform heating. Non-uniform heating is well distinguished in EOF_1 but is no longer visible on later EOFs. Defect visibility is improved with respect to the uncorrected case; it is possible now to detect 24 of the 25 inclusions with EOF_2 to EOF_5, and the fiber matrix can be seen in EOF_2.

5. THE HOUGH TRANSFORM

5.1. Theory

The Hough transform [16] is a standard tool in image analysis that allows recognition of patterns in an image by finding geometrical structures that can be parameterized as straight lines, polygons, circles, etc. It is based on the polar representation of a straight line (in Cartesian coordinates: $y=mx+b$), which is given by [9, 17]:

$$\rho = x\cos\theta + y\sin\theta \tag{6}$$

where ρ is the radius and θ is the angle of a normal to the line of origin. The pair (ρ,θ) defines a vector from the origin to the nearest point of the line. Eq. (6) can be used, however the `hough(…)` function in MATLAB® greatly speed up the calculations.

Any pattern in the *x-y* space can be transformed to a parametric ρ - θ space, or *Hough* space. For instance, any line in the *x-y* plane corresponds to a dot in the ρ-θ space, and any point in the *x-y* plane corresponds to a sinusoidal curve in the ρ - θ space. Hence, each single point that lies on a straight line in the Cartesian space as the black markers (A, B, C, D, E, F) in Figure 10a, plot to a sinusoidal curve in the Hough space, as in Figure 10b, and all of these curves must intersect at a point (ρ_0,θ_0) representing the line they all have in common [9]. If a second set of points (white markers denoted as a, b, c, d, e, f) are located randomly in such a way that they perfectly fit the same straight line, their corresponding sinusoidal counterparts in the Hough space will approximately intersect at the same point, as in Figure 10c.

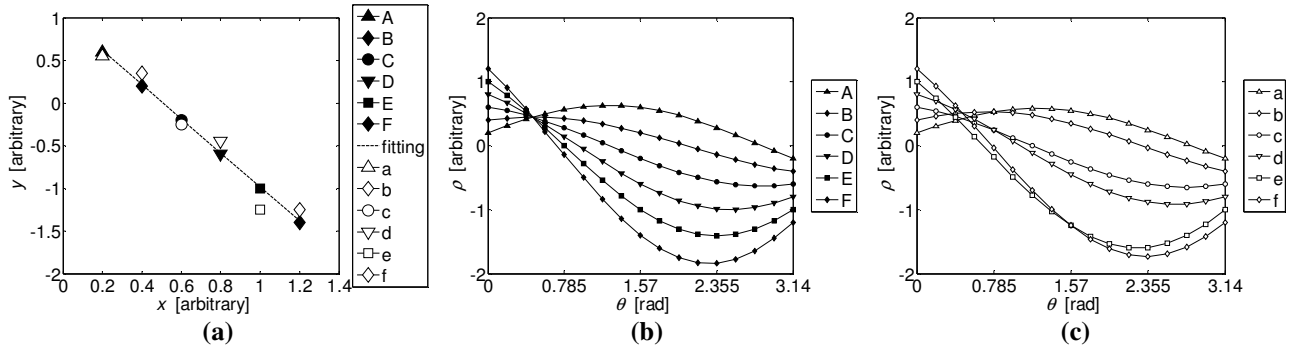

Figure 10. (a) Six points forming a perfect (black) and an approximated (white) straight line in the Cartesian space; and the Hough space representation for the six (b) black (A, B, C, D, E, F); and (c) white points (a, b, c, d, e, f).

The distribution of points around the intersection point in the Hough space provides an indication of the goodness of the fitting in the Cartesian space. There are two interesting applications of the HT to thermography as explained next.

5.2. Analysis of pulsed thermographic sequences

Thermal profiles from a PT experience present a typical behavior. Figure 11 shows an example for a Plexiglas® plate with 6 flat-bottom holes of different depths on the rear side. Temperature for a non-defective pixel can be modeled approximately with the 1D solution of the Fourier equation for a homogeneous semi-infinite plate, *i.e.* temperature will decay following a -0.5 slope on a logarithmic scale. On the contrary, defective pixels will diverge from this behavior at a given instant, which is related to its depth (see Figure 11a). The HT can be used to identify the pixels from a thermogram sequence that follow this -0.5 slope in time. To do so, the HT is applied pixel-wise to the entire sequence. From Eq. (6) and with $m=-\cos(\theta)/\sin(\theta)$, the region of interest in the Hough space is located around an angle $\theta\approx1.1071$ rad [3]. Analyzing the distribution of points in the $\theta\approx1.1071$ rad column (see Figure 11b), it is possible to determine statistically if a pixel belongs to a non-defective or a defective area.

The Hough space can be seeing as an accumulator that sums up the votes of all pixels in the sequence. Since every point in the Cartesian space will produce a sinusoid in the Hough space, and each point along this sinusoid will get a vote added to each point in the real space, the crossing points in the Hough space will provide an indication of the location of

the local maxima that define a straight line. The histogram distribution for a non-defective area shows a sharp decay (when compared to a defective area, see Figure 11c) that can be modeled by an exponential function of the form [3]:

$$\xi(x) = a \exp\left[\left(\frac{x-b}{c}\right)^2\right] \tag{7}$$

As noted in [3], parameters a and c are highly correlated to the depth of the defect, the deeper the defect the broader the histogram distribution (see Figure 11c), and can be used to determine whether a pixel is part of a defective or non-defective area and also to have a good idea of its relative depth.

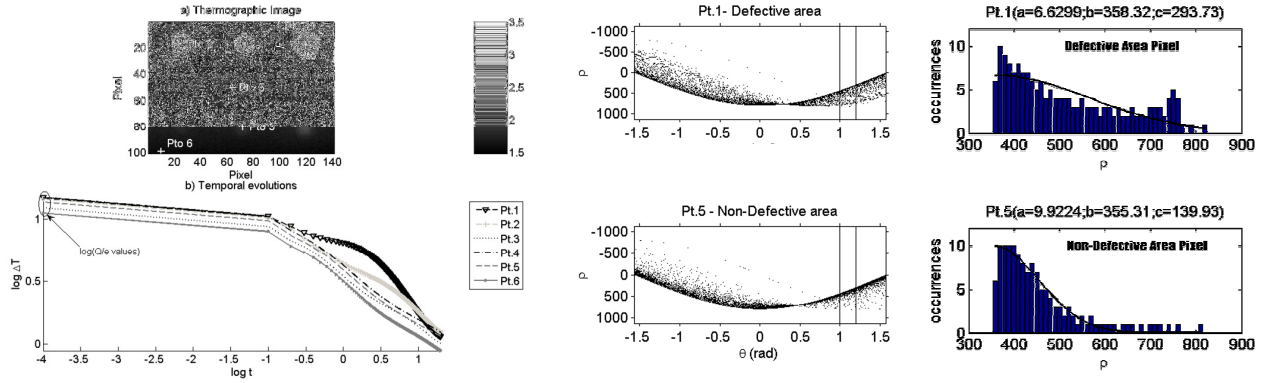

(a) **(b)** **(c)**

Figure 11. Plexiglas® specimen with 6 flat-bottom holes at different depths: (a) thermogram (top) showing 6 selected locations and their corresponding thermal profiles (bottom); (b) Hough space for points 1 (defective) and 5 (non-defective); and (c) corresponding histogram distribution of the values in column $\theta \approx 1.1071$ rad. Data from [3].

5.3. Differentiated absolute phase contrast

The HT can also be applied on PPT experiences provided that data has been adequately sampled and truncated and that enough information is available at high frequencies. As portrayed in Figure 3, phase profiles have an approximately linear behavior between the blind frequency and the maximum available frequency. Hence, the HT can be used to identify the blind frequency (*i.e.* f_b) without the need of selecting a sound area. The process has been automated [4], the final result of the so-called differentiated absolute phase contrast (DAPhC) is a blind frequency image (Figure 12a) that can be used to extract the depth information as shown in Figure 12b for the Plexiglas® plate described above.

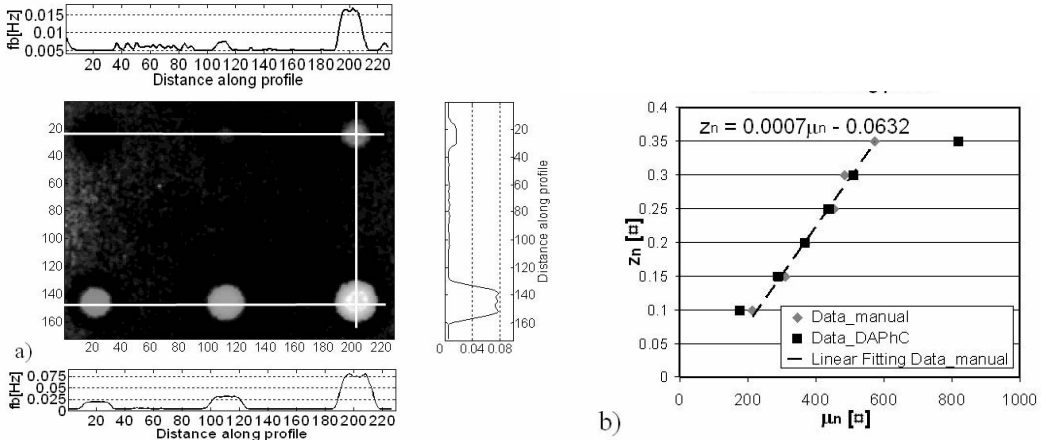

Figure 12. (a) Blind frequency image; and (b) correlation between depth and blind frequency. Data from [4].

6. THE LAPLACE TRANSFORM

6.1. Theory

The Laplace transform (LT) is commonly used to reduce the problem of solving differential equations to an algebraic problem. In this way, instead of looking for an analytical solution in the *original* space, it is possible to solve the problem in the *Laplace* space, which hopefully will exhibit an explicit form (and often does) and thus, providing a physical insight of the problem in hand. Interestingly, initial value problems are solved without first determining a general solution and then transformed back to the original space. This concept is not new. For instance, Carslaw proposed in 1921 to replace the heat diffusion equation and its initial boundary conditions by a linear matrix equation linking the input and output vectors in the Laplace space [20], though it was not until recently that appropriate inversion tools and computer power were available to actually implement this. The LT is a valuable instrument for solving the direct and inverse problems of one or multi-dimensional diffusion within a multilayer composite containing one or several defects as described next.

6.2. Using the continuous Laplace transform to solve the direct problem in 1D heat diffusion

Figure 13 illustrates the problem of heat diffusion through a slab having two composite layer of thickness e_1 and e_2 ($e=e_1+e_2$ is the total thickness), submitted to a Dirac heat pulse $\delta(t)Q$. A delamination is located between the two layers, and is characterized by a thermal resistance R_c. The temperature at the front and rear surfaces are denoted T_f and T_r, respectively. The Laplace transform of T_f and T_r, *i.e* the *Laplace temperatures* θ_f and θ_r, can be derived using thermal quadrupoles [21].

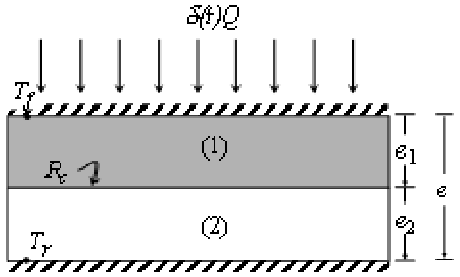

Figure 13. Bi-layer composite of thickness e ($e=e_1+e_2$), with a delamination of a thermal resistance R_c, submitted to a Dirac heat pulse $\delta(t)Q$.

The quadrupole matrix equation will have the following form for the two layer slab considered in Figure 13:

$$\begin{bmatrix} \theta_f \\ Q \end{bmatrix} = \begin{bmatrix} A_1 & B_1 \\ C_1 & A_1 \end{bmatrix} \begin{bmatrix} 1 & R_c \\ 0 & 1 \end{bmatrix} \begin{bmatrix} A_2 & B_2 \\ C_2 & A_2 \end{bmatrix} \begin{bmatrix} \theta_r \\ 0 \end{bmatrix} \tag{8}$$

where subscripts 1 and 2 corresponds to the first and second layers of the material, respectively and:

$$A_j = \cosh\left(e_j\sqrt{p/\alpha}\right)\ ;\quad B_j = 1/\left(k\sqrt{p/\alpha}\right)\sinh\left(e_j\sqrt{p/\alpha}\right)\ ;\quad C_j = \lambda_x\sqrt{p/\alpha}\sinh\left(e_j\sqrt{p/\alpha}\right) \tag{9}$$

where j is 1 or 2 (for each layer); the thermal diffusivity α and the conductivity k are taken only in the transverse direction since heat diffusion is 1D, and p is the Laplace variable. Reference [5] provides some guidelines for the correct determination of p.

After algebraic manipulation (see [21] for details), the Laplace thermal contrast for the reflection and transmission modes can be written as:

$$\Delta\theta_{reflection} = \theta_f - \theta_{Sa,f} = \frac{QR_c\sinh^2\left(e_2\sqrt{p/\alpha}\right)}{\sinh\left(e\sqrt{p/\alpha}\right)\cdot\left[\sinh\left(e\sqrt{p/\alpha}\right)+k\sqrt{p/\alpha}\cdot R_c\sinh\left(e_1\sqrt{p/\alpha}\right)\cdot\sinh\left(e_2\sqrt{p/\alpha}\right)\right]} \tag{10}$$

$$\Delta\theta_{transmission} = \theta_r - \theta_{Sa,r} = \frac{QR_c\sinh\left(e_1\sqrt{p/\alpha}\right)\sinh\left(e_2\sqrt{p/\alpha}\right)}{\sinh\left(e\sqrt{p/\alpha}\right)\cdot\left[\sinh\left(e\sqrt{p/\alpha}\right)+k\sqrt{p/\alpha}\cdot R_c\sinh\left(e_1\sqrt{p/\alpha}\right)\cdot\sinh\left(e_2\sqrt{p/\alpha}\right)\right]} \tag{11}$$

where $\theta_{Sa,f}$ and $\theta_{Sa,r}$ are the Laplace transforms of the reference temperature (sound area, S_a) on the front and rear faces, respectively. Eqs. (10) and (11) are explicit equations that can be use to solve the inverse problem as explained next.

6.3. Using the discrete Laplace transform to solve the inverse problem

Having developed an expression for the LT of the signal in the transformed space, it is now possible to derive explicit inversion solutions. The discrete Laplace transform can be written in its dimensionless form as follows [22]:

$$m(p^*) = \sum_{i=1}^{i_{\max}} \Delta T(t_i^*) \exp\left(-p^* t_i^*\right) \Delta t^* \tag{12}$$

with the dimensionless parameters (denoted with an *) defined as:

$$t^* = \frac{\alpha t}{e^2} \quad ; \quad p^* = \frac{e^2 p}{\alpha} \tag{13}$$

There are three definitions for the thermal contrast depending on the situation: ΔT_{trans} is used for the transmission case, $\Delta T_{ref,short}$ is convenient for the reflection mode when the thermal profiles do not reach stabilization (*e.g.* low conductivity materials and/or short acquisition times); and $\Delta T_{ref,long}$ is preferred for the reflection mode when a stabilization temperature is attained (*e.g.* high conductivity materials and/or long acquisition times):

$$\Delta T_{trans} = \frac{T}{T_{\max}} - \frac{T_{Sa,r}}{T_{Sa,r,\max}} \quad ; \quad \Delta T_{ref,short} = \frac{1}{\sqrt{\pi\, t_s}} \left(\frac{T}{T_{ERT}} - \frac{T_{Sa,f}}{T_{Sa,f,ERT}} \right) \quad ; \quad \Delta T_{ref,long} = \frac{T}{T_{LRT}} - \frac{T_{Sa,f}}{T_{Sa,f,LRT}} \quad ; \tag{14}$$

Eq. (12) can be applied pixel by pixel resulting in a unique image for every value of the reduced Laplace variable p^*. With this information, it is now possible to derive an explicit solution for the dimensionless thermal resistance R_c^* and for the dimensionless depth z of a defect, respectively [5, 22]:

$$R_c^* = \frac{m_1^2 \left[1 + 2\sqrt{p^*} \sinh\left(2\sqrt{p^*}\right) m_2 \right] \cdot \sinh\left(\sqrt{p^*}\right) \tanh\left(\sqrt{p^*}\right)}{\left[1 + \sqrt{p^*}\, m_1 \cdot \sinh\left(\sqrt{p^*}\right) \right] \cdot \left[-m_1 + m_2 \cdot \cosh\left(\sqrt{p^*}\right) - 3\sqrt{p^*}\, m_1 m_2 \cdot \sinh\left(2\sqrt{p^*}\right) \Big/ 2 \right]} \tag{15}$$

$$z = 1 - \frac{1}{\sqrt{p}} \ln\left[\left(\frac{m_2}{m_1} \right)^{1/2} \cosh\left(p^{-1/2}\right) + \left(\frac{m_2}{m_1} \cosh^2\left(p^{-1/2}\right) - 1 \right)^{1/2} \right] \tag{16}$$

where m_1 and m_2 are the LT for p^*_1 and p^*_2 (p^*_2=4 p^*_1), respectively, R^*_c= R_c/(*e*/*k*) and z^*=*z*/*e*.

Eqs. (15) and (16) rely on a 1D heat conduction model. Nevertheless, the 2D and 3D cases have also been addressed by implementing a Fourier transformation after the Laplace transform leading to an analytical expression in terms of a *Laplace-Fourier* (2D case), or a *Laplace-Fourier-Fourier* space (3D case). Figure 14 shows an example of application using perturbation modeling in transient 3D heat transfer on a 60x60x2 mm^3 14 layer CFRP slab with a 10x10 mm^2 Teflon® 25 µm inclusion at the center [5]. The estimated resistance for this case, using Eq. (15), was R^*_c =0.185, which is ~153% higher than the actual value of R^*_c =0.073. Two causes for this deviation were identified [5]: the high noise levels and the presence of trapped air between CFRP and Teflon® layers.

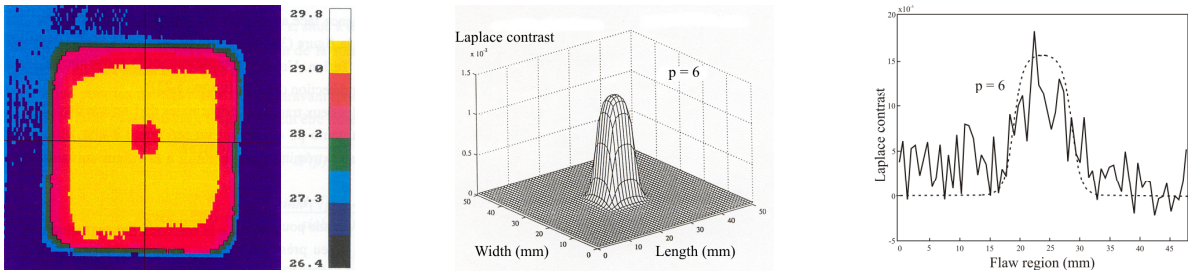

(a) **(b)** **(c)**

Figure 14. (a) Thermogram at *t*=2s, (b) theoretical Laplace distribution calculated for *z*=0.5 mm; and (c) experimental Laplace profile (continuous) with theoretical profile (dotted line) superimposed for comparison. Data from [5].

7. CONCLUSIONS

A wide variety of transformation algorithms can be applied to thermographic pulsed data in order to analyze the information in an alternative space. The Fourier transform constitutes without a doubt the most commonly used transform in signal processing. The FT uses sinusoids as basis functions to decompose the signal from the *temperature-time* space to a *phase or amplitude-frequency* space. The phase have proven to be very useful not only for qualitative but also for quantitative analysis. Although the use of oscillatory waves is very convenient in order to extract amplitude and phase delay information, it may not be the optimal choice to correctly represent transient signals (as the temperature profiles typically found in pulsed thermography). The use of waves of limited duration, or *wavelets*, constitutes an interesting alternative. The results presented here using the wavelet transform demonstrate the potential of wavelets for depth inversion. Efforts are now directed to an optimal selection of the mother wavelet in order to increase time resolution at early times. Instead of defining a basis function, another possibility is to use statistical modes to discriminate spatial and temporal information. Singular value decomposition provides a compact representation of data by sorting the spatial information as a set of empirical orthogonal functions (EOFs) and time information as a set of principal components (PCs). We presented the case of a CFRP specimen for which defect visibility was considerably enhanced even for unprocessed data.

The Hough transform is another standard transform in signal processing that can be used with thermographic data but in a different way. It is possible to detect lines (and other geometrical forms) through the HT. Two applications were described here: an automation algorithm for defect detection from thermal profiles, and a procedure for the automatic detection of the blind frequencies from a phase profile.

We concluded with the Laplace transform, which can be used to solve the direct and the inverse problem for one or multidimensional heat conduction. We illustrated this approach for the case of a bi-layer composite material.

The progressive and continuous increase in computer power together with the availability of transformation tools within most common software commercial packages encourages further developments in the field. For instance, a Hough transform module was added in the latest release of MATLAB® (v. 7) dramatically reducing the calculation times from several hours using Eq. (5), to several minutes using the `hough(...)` function, and there is still room for improvement.

REFERENCES

1. Maldague X. P. and Marinetti S. “Pulse phase infrared thermography,” *J. Appl. Phys*., **79**(5):2694-2698, 1996.
2. Galmiche F. and Maldague X. “Depth defect retrieval using the wavelet pulsed phased thermography,” *Proc. 5th Conference on Quantitative InfraRed Thermography (QIRT)*, Eurotherm Seminar 64, D. Balageas, G. Busse, C. Carlomagno (eds.), Reims, France, July 18-21, 2000, 194-199.
3. González D. A., C. Ibarra-Castanedo, López-Higuera J. M. and Maldague X. “New algorithm based on the hough transform for the analysis of pulsed thermographic sequences,” *Proc. V International Workshop Advances in Signal Processing for Non Destructive Evaluation of Materials (IWASPNDE)*, Quebec, 2005, *in press*.
4. González D. A., Ibarra-Castanedo C., Madruga F. J. and Maldague X. “Differentiated absolute phase contrast algorithm for the analysis of pulsed thermographic sequences,” *Infrared Phys. & Technol., in press*.
5. Bendada, A. Erchiqui F. and Lamontagne M. “Pulsed thermography in the evaluation of an aircraft composite using 3D thermal quadrupoles and mathematical perturbations,” *Inverse Problems*, **21**(3):857-877, 2005.
6. Rajic N. “Principal component thermography for flaw contrast enhancement and flaw depth characterization in composite structures,” *Compos. Struct*., **58**:521-528, 2002.
7. Bracewell R. The Fourier Transform and its Applications, McGraw-Hill, USA, 1965.
8. Brighman E. O. *The Fast Fourier Transform*, Prentice-Hall, Inc., Englewood Cliffs, N. J., 1974.
9. Castleman K. R. *Digital Image Processing*, Prentice-Hall, Upper Saddle River, N. J. 1996.
10. Busse G. and Rosencwaig A. “Subsurface imaging with photoacoustics,” *Appl. Phys. Lett.*, **36**(10):815-816, 1980.
11. Meola C. and Carlomagno G. M. “Recent advances in the use of infrared thermography”, *Meas. Sci. Technol.,* **15**:27–58, 2004.

12. Ibarra-Castanedo C. “Quantitative subsurface defect evaluation by pulsed phase thermography: depth retrieval with the phase,” *Ph. D. Thesis*, Laval University, [available online: http://www.theses.ulaval.ca/2005/23016/23016.pdf].
13. Ibarra-Castanedo C. and Maldague X. “Interactive Methodology for Optimized Defect Characterization by Quantitative Pulsed Phase Thermography,” *Res. Nondestr. Eval.,* **16**(4): 1-19, 2005.
14. Ibarra-Castanedo C., Avdelidis N. P. and Maldague X. “Quantitative assessment of steel plates using pulsed phase thermography,” *Mater. Eval.,* **63**(11):1128-1133, November 2005.
15. Sheng, Y. “Wavelet Transform” in *The transforms and applications handbook*, 2nd edition, Alexander D. Poularikas (ed.), Boca Raton: CRC Press LLC, 2000.
16. Hough P. Method and means for recognizing complex patterns, U. S. Patent 3069654, 1962.
17. Russ J. C. *The image processing handbook*, 4th edition, CRC Press LLC, Boca Raton, FL, 2002.
18. Ibarra-Castanedo C., Bendada A. and Maldague X. “Image and signal processing techniques in pulsed thermography,” *GESTS Int'l Trans. Computer Science and Engr.,* **22**(1):89-100, November 2005.
19. Marinetti S., Grinzato E., Bison P. G., Bozzi E. Chimenti M. Pieri G. and Salvetti O. “Statistical analysis of IR thermographic sequences by PCA,” *Infrared Phys. & Technol.*, **46**:85-91, 2004
20. Carslaw H. S. Introduction to the mathematical theory of heat in solids, Macmillan, 1921.
21. Maillet D., André S., Batsale J. C., Degiovanni A. and Moyne C. *Thermal Quadrupoles: Solving the heat equation through integral transforms*, John Wiley & Sons, Ltd., West Sussex, England, 2000.
22. Maillet D., Batsale J.-C., Bendada A. and Degiovanni A. “Méthodes intégrales et contrôle non destructif par thermographie infrarouge,” *Rev. Gén. Therm.*, **35**:14-27, 1996.